Available online at www.sciencedirect.com
ScienceDirect
Icarus ••• (••••) •••–•••
ICARUS
www.elsevier.com/locate/icarus

# Equilibrium rotational stability and figure of Mars

Amy Daradich [a], Jerry X. Mitrovica [a,*], Isamu Matsuyama [b], J. Taylor Perron [c], Michael Manga [d], Mark A. Richards [d]

[a] *Department of Physics, University of Toronto, 60 St. George Street, Toronto, M5S 1A7 Canada*
[b] *Department of Terrestrial Magnetism, Carnegie Institution of Washington, 5241 Broad Branch Road NW, Washington, DC 20015, USA*
[c] *Department of Earth and Planetary Sciences, Harvard University, 20 Oxford St., Cambridge, MA 02138, USA*
[d] *Department of Earth and Planetary Sciences, University of California, Berkeley, CA 94720-4767, USA*

Received 20 May 2007; revised 4 October 2007

**Abstract**

Studies extending over three decades have concluded that the current orientation of the martian rotation pole is unstable. Specifically, the gravitational figure of the planet, after correction for a hydrostatic form, has been interpreted to indicate that the rotation pole should move easily between the present position and a site on the current equator, 90° from the location of the massive Tharsis volcanic province. We demonstrate, using general physical arguments supported by a fluid Love number analysis, that the so-called non-hydrostatic theory is an inaccurate framework for analyzing the rotational stability of planets, such as Mars, that are characterized by long-term elastic strength within the lithosphere. In this case, the appropriate correction to the gravitational figure is the equilibrium rotating form achieved when the elastic lithospheric shell (of some thickness *LT*) is accounted for. Moreover, the current rotation vector of Mars is shown to be stable when the correct non-equilibrium theory is adopted using values consistent with recent, independent estimates of *LT*. Finally, we compare observational constraints on the figure of Mars with non-equilibrium predictions based on a large suite of possible Tharsis-driven true polar wander (TPW) scenarios. We conclude, in contrast to recent comparisons of this type based on a non-hydrostatic theory, that the reorientation of the pole associated with the development of Tharsis was likely less than 15° and that the thickness of the elastic lithosphere at the time of Tharsis formation was at least ∼50 km. Larger Tharsis-driven TPW is possible if the present-day gravitational form of the planet at degree 2 has significant contributions from non-Tharsis loads; in this case, the most plausible source would be internal heterogeneities linked to convection.


*Keywords:* Rotational dynamics; Mars

## 1. Introduction

A diverse set of studies have argued that the rotation pole of Mars has been subject to large excursions relative to the surface geography, or true polar wander (TPW), including 90° reorientations known as inertial interchange events. The observations supporting these studies include equatorial deposits that resemble sediments at the present poles of Mars (Schultz and Lutz, 1988), hydrogen rich equatorial deposits which are inferred to be remnants of ancient polar caps (Wieczorek et al., 2005) and analyses of crustal magnetic anomalies that suggest an early magnetic field existed that is not aligned with the current rotation axis (Arkani-Hamed and Boutin, 2004; Hood et al., 2005). Other geological evidence for significant TPW on Mars is found in the spatial distribution of valley networks that appear to be formed by liquid surface runoff (Mutch et al., 1976) and craters formed by oblique impacts, which may record the demise of ancient equatorial satellites (Schultz and Lutz-Garihan, 1982).

The most prominent feature in the geology of the martian surface is the Tharsis rise. The figure of Mars, as defined by the gravitational potential field of the planet, is dominated by the signature of this massive volcanic structure (Smith et al., 1999) and a rotationally-induced equatorial bulge. Previous analyses of this figure have commonly focused on two questions related to the stability and evolution of the mar-

* Corresponding author. Fax: +1 (416) 978 7606.
*E-mail address:* jxm@physics.utoronto.ca (J.X. Mitrovica).

0019-1035/$ – see front matter 
doi:10.1016/j.icarus.2007.10.017

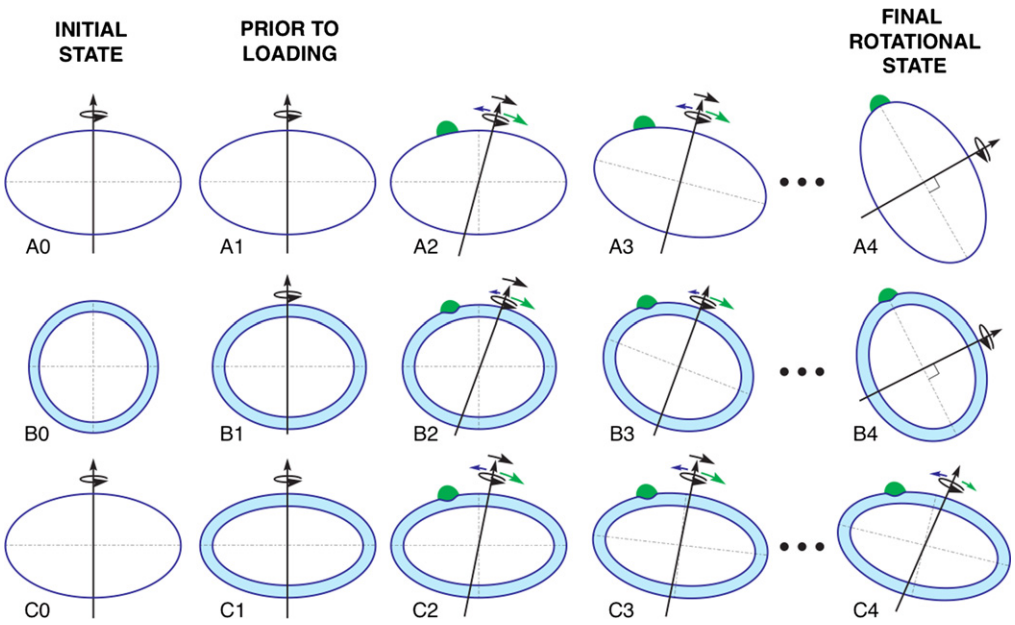


Fig. 1. Schematic illustration highlighting the physics of TPW. (A) The scenario described by Gold (1955) in which an initially hydrostatic planet (A0, A1) is subject to a surface mass load (green beetle, A2) which is assumed to remain partially uncompensated. The load will push the pole away (green arrow), while the hydrostatic rotational bulge will, initially, resist this tendency (blue arrow). However, this resistance will disappear as the hydrostatic rotational bulge relaxes completely to the new rotational state (A3), leading to further load-induced TPW. The process will continue until the load eventually reaches the equator (A4). (B) The rotational stability of an initially spherical and non-rotating planet (B0) with an elastic lithosphere (blue shell) subject to a surface mass loading. Once the model planet is set rotating, it will ultimately achieve the equilibrium form shown in B1. As in (A), the application of a surface mass load will move the pole away, though this motion is initially resisted by the equilibrium rotational bulge (B2). The equilibrium rotational bulge will eventually reorient perfectly to the new rotation vector (i.e., the equilibrium rotational bulge in B3 is identical to that of B1) and TPW will proceed without memory of the previous rotational state. Eventually, as in (A), TPW will cease when the load reaches the equator (B4). (C) The scenario described by both Willemann (1984) and Matsuyama et al. (2006), in which an initially hydrostatic planet (C0) develops an elastic shell through cooling of the interior (C1). The shell develops without any internal elastic stresses and thus the form of the planet will be identical to the hydrostatic case in A1 rather than to the (less oblate) equilibrium form in B1. The appearance of a surface mass load will act to push the pole away, and this will be resisted by the rotational bulge. However, in contrast to the first two cases, in this scenario the bulge cannot perfectly adjust to the new rotation axis (note that the oblate form in C3 is not symmetric relative to the rotation axis) since the shell had an initially hydrostatic form (C1), while TPW introduces elastic stresses within the shell. This incomplete adjustment, which introduces a memory of the original rotational state, is referred to as the remnant rotational bulge (Willemann, 1984), and it acts to stabilize the pole. Ultimately, the load will not reach the equator (C4), but rather a position governed by the balance between the load-induced push and the pull associated with the remnant rotational bulge. Note that if one removed the load in A4 and B4, the pole would not move; however, this removal would cause the pole in C4 to return to its original orientation (C1). For each scenario, the figures are drawn so that the $z$-axis is fixed to the initial rotation pole in order to be consistent with the mathematical analysis appearing in the appendix. The figure could also have been drawn so that the rotation axis at any time coincided with the $z$-axis; the evolving geometry in this case would be essentially consistent with the view of an inertial observer.

tian rotation vector. First, to what extent did the development of Tharsis, which is now located near the equator of the planet (Zuber and Smith, 1997), cause TPW (Melosh, 1980; Sprenke et al., 2005)? Second, how stable is the current rotation axis to changes in the surface and internal mass distribution (Bills and James, 1999)?

In an important conceptual study, Gold (1955) discussed the rotational stability of a simple, 'hydrostatic' planet subject to a surface mass loading (see Fig. 1A). A surface load will act to push the pole away. In the short term, the rotational bulge will resist this tendency and stabilize the rotation axis (Fig. 1A2). However, in the long term the bulge will relax completely (i.e., hydrostatically) to any reorientation of the pole position (Fig. 1A3), thus erasing all memory of past positions, and permitting further load-induced TPW. Eventually, the load, even one as small as Gold's famous beetle, will reach the equator (Fig. 1A4), the minimum energy state of the system. That is, TPW will continue until the pole aligns with the maximum axis of inertia associated with any surface load (i.e., non-hydrostatic) forcing. [Note that the Gold (1955) scenario includes a physical inconsistency since it assumes that the rotational bulge will relax perfectly to a change in centrifugal potential but that the surface load is never completely compensated isostatically.] It remains a common view, following Gold's influential analysis, that the stability of the martian rotation pole—both at present day and in response to Tharsis loading—is governed by the observed figure of the planet after correction for a hydrostatic form (Melosh, 1980; Bills and James, 1999; Sprenke et al., 2005).

In this context, a series of studies since 1980 have reached the conclusion that the present non-hydrostatic form of Mars (i.e., the form which results from removing the figure predicted on the basis of the present-day rotation vector in the case where there are no viscous or elastic stresses) is characterized by a maximum axis of inertia that lies along the current equator, 90° from Tharsis, while the intermediate axis of inertia is aligned with the present-day pole (Melosh, 1980; Bills and James, 1999). The more recent of these analyses demonstrate that the maximum and intermediate non-hydrostatic moments of inertia are nearly equal (e.g., Bills and James, 1999), and thus

Please cite this article in press as: A. Daradich et al., Equilibrium rotational stability and figure of Mars, Icarus (2007), doi:10.1016/j.icarus.2007.10.017

conclude that the current rotation vector of Mars is inherently unstable. That is, relatively small surface mass loads can cause large (order 90°) excursions of the pole along the great circle joining the present-day pole and the maximum non-hydrostatic inertia axis. Furthermore, analysis of the non-hydrostatic form, after correction for the signal from Tharsis loading, has led to a conclusion that the development of this volcanic province must have induced a large (15°–90°) excursion of the rotation pole (Sprenke et al., 2005).

The incomplete isostatic compensation of the ancient Tharsis load implies that Mars is characterized by non-zero long-term strength within the lithosphere (Zuber and Smith, 1997), and estimates of the elastic thickness of this region range up to several hundred kilometers (McGovern et al., 2004; Zhong and Roberts, 2003; Turcotte et al., 2002; Sohl and Spohn, 1997). The question then arises: Is the non-hydrostatic stability theory cited above valid for a planet with an elastic lithosphere? [This question was also posed, without resolution, by Bills and James (1999, p. 9094).]

Willemann (1984) recognized that the presence of an elastic shell has a potentially significant stabilizing effect on TPW. However, his analysis, recently refined and corrected by Matsuyama et al. (2006), has been neglected in subsequent studies of Mars' rotational stability (Bills and James, 1999; Sprenke et al., 2005). There may be two reasons for this neglect. First, Willemann (1984), and also Matsuyama et al. (2006), considered the general problem of load-induced TPW, with some emphasis on Mars and Tharsis, but they did not quantitatively address the implications of their results for the present-day figure of the planet. Second, Willemann (1984) and Matsuyama et al. (2006) analyzed a specific scenario in which a lithosphere develops through cooling of an initially hydrostatic planet which is then subject to loading (see below). In any event, the Willemann (1984) study indicates that a non-hydrostatic theory for rotational stability is not appropriate for a planet that has a sufficiently thick elastic lithosphere (e.g., Mars; see also the discussion on p. 28,682 of Zuber and Smith, 1997).

Accordingly, the main goal of this paper is to derive, using physical arguments supported by standard mathematical analysis, a new, generalized statement of rotational stability that is valid for any planet—whether it has an elastic lithosphere or not. With this generalization in hand, we first reassess the level of present-day rotational stability implied by Mars' gravitational figure. Next, we extend the analysis of Matsuyama et al. (2006) to quantify the total contribution of load-induced TPW to the planetary figure. Finally, we compare these new expressions to observational constraints on the figure of Mars in order to set bounds on the range of Tharsis-induced TPW.

## 2. The physics of rotating planets

In this section we will discuss the physics of load-induced TPW on planetary models that are characterized by the presence or absence of a uniform elastic lithosphere (Fig. 1). In the former case, the thickness of the lithosphere is denoted by $LT$. Our discussion will be supported by the mathematical analysis appearing in Appendix A, which is based on standard fluid Love number theory. That is, we consider time scales long enough such that all viscous stresses associated with the response to surface mass loading and changes in the rotational (i.e., centrifugal) potential have relaxed completely.

As we discussed in reference to Fig. 1A, Gold (1955) was concerned with the rotational stability of a planet in purely hydrostatic equilibrium. Such a planet has no elastic strength ($LT = 0$), and in this case the rotational flattening (or oblateness) of the background hydrostatic form (Fig. 1A0 or 1A1) is a function of the rotation rate, $\Omega$, and the internal density structure of the planet [Eq. (A.11); the sensitivity to internal structure is embedded within the fluid tidal $k$ Love number computed for the model with no lithosphere, $k_f^{T,*}$]. In this scenario, any non-hydrostatic contributions to the inertia tensor will be associated with the applied surface mass load [Eq. (A.9)]. Thus, diagonalization of the non-hydrostatic inertia tensor will yield a maximum principal axis (or rotation pole) that is oriented 90° from the load, as in Fig. 1A4. The minimum principal axis will pass through the center of the load, and both the intermediate and minimum axes will pass through the equator.

Next, we turn to scenarios in which the planet has an elastic lithosphere, beginning with Fig. 1B. In this somewhat unrealistic, but nevertheless physically instructive case, an initially non-rotating planet with a pre-existing elastic lithosphere (Fig. 1B0) is spun-up to its current rotation rate, and the system is allowed to reach a state in which all sub-lithosphere viscous stresses relax completely (Fig. 1B1). This relaxed form will not be in hydrostatic equilibrium, since the elastic lithosphere has permanent strength, and thus the oblateness of the form will be less than the hydrostatic flattening in Fig. 1A (Mound et al., 2003). To distinguish the former from the latter we will henceforth use the term 'equilibrium form,' and note that this form approaches the hydrostatic figure as the elastic lithospheric thickness approaches zero. Mathematically, the oblateness of the equilibrium form is a function of the rotation rate, $\Omega$, and the fluid tidal $k$ Love number, $k_f^T$ [Eq. (A.16)], and the latter is a function of both the internal density structure of the planet and the thickness of the elastic lithosphere ($k_f^T \to k_f^{T,*}$ from below as $LT \to 0$) (Mitrovica et al., 2005; Matsuyama et al., 2006).

As in Fig. 1A, a load applied to this model planet will ultimately reach the equator (Fig. 1B4) since the equilibrium rotational bulge which defines the initial rotating state (Fig. 1B1) will eventually reorient perfectly to a change in the position of the rotation pole [i.e., it provides no memory of a previous rotational state; see figure caption and the discussion between Eqs. (A.12) and (A.14)]. However, it would be incorrect to analyze the rotational stability of this system using non-hydrostatic stability theory. Specifically, if one were to correct the figure in Fig. 1B1 for a hydrostatic form, one would be left with a residual, non-hydrostatic form that was characterized by a deficit in oblateness, or mass excess at the poles, i.e., a prolate spheroid. (Mathematically, this difference arises because $k_f^T < k_f^{T,*}$ when $LT \neq 0$.) One would thus erroneously introduce a spurious tendency for the entire figure to drive a TPW event that would

move the pole towards a point on the current equator, 90° from Tharsis.

We conclude that the long-term stability of a rotating planet is governed by the terms in the inertia tensor which do not perfectly reorient to the contemporaneous rotation axis [Eq. (A.13)]. That is, the hydrostatic form in the scenario of Fig. 1A [Fig. 1A1; Eq. (A.8)] and the equilibrium form in the scenario of Fig. 1B [Fig. 1B1; Eq. (A.13)] are irrelevant to the long-term rotational stability. Thus, the stability of the system in Fig. 1B is governed by the non-equilibrium (rather than non-hydrostatic) inertia tensor. This statement provides a fundamental extension of the Gold (1955) stability theory to the case of planets, like Mars, with non-zero (very long-term) elastic strength in the lithosphere.

Fig. 1C shows a more complicated and realistic scenario for such planets that has been considered by both Willemann (1984) and Matsuyama et al. (2006). An initially hydrostatic, rotating planet (Fig. 1C0) cools and develops a uniform and unbroken elastic lithosphere (Fig. 1C1). Lithospheric formation will not disturb the hydrostatic form since the elastic lithosphere will grow in a fully relaxed state. In contrast to Fig. 1B (or Fig. 1A), the rotational bulge cannot reorient perfectly to a change in the pole position since there would be no way for the elastic lithosphere to re-establish a hydrostatic form around the new pole position: TPW will introduce stresses in the previously stress-free lithosphere. The system thus has a memory of the initial rotational state (Fig. 1C1) and any departures from this state would be resisted. The final load position (Fig. 1C4), which is not at the equator, represents a balance between this resistance and the tendency of the load to drive TPW. Unless the load is of the same order of magnitude as the mass associated with the rotational bulge, little TPW can occur.

Is our generalized statement that rotational stability is governed by non-equilibrium components of the inertia tensor appropriate to the scenario depicted in Fig. 1C? To answer this requires that we separate the change in shape between the initial (Fig. 1C1) and final (Fig. 1C4) rotational states into a contribution that perfectly reorients as the pole moves around and a residual term. Physically, the latter can be inferred by simply switching off rotation in the case of Fig. 1C1 and determining the departure from sphericity that would result. This departure would be the difference between the hydrostatic form (Fig. 1C1) and the equilibrium form associated with a planet having the same rotation rate and elastic lithospheric thickness (as in Fig. 1B1). This difference, which is termed the remnant rotational bulge (Willemann, 1984; Matsuyama et al., 2006), is frozen into place relative to the initial pole position. Thus the oblateness in Fig. 1C1 can be decomposed into a component from the remnant rotational bulge, which stays fixed relative to the initial rotation axis, and an equilibrium rotational form that will adjust perfectly (in the long-time limit) as the pole moves from the initial to final (Fig. 1C4) state. Therefore, as in Fig. 1B, the rotational stability of the planet is governed by non-equilibrium components of the inertia tensor. As in previous scenarios, these components include the surface mass load, but, in the case of Fig. 1C they also include a remnant bulge.

The same separation of the figure of the planet into: (1) an equilibrium form that adjusts perfectly to the change in the orientation of rotation and thus has no bearing on the rotational stability; and (2) a non-equilibrium, remnant rotational form oriented with the initial pole position, is derived mathematically in Appendix A.1.3 [see Eqs. (A.19) to (A.21)].

As a final point, Matsuyama et al. (2007) have analyzed the rotational stability of the scenario in Fig. 1C by writing expressions for the total energy in the system and finding the TPW that minimizes this energy. Their expressions provide an independent confirmation that it is the diagonalization of the non-equilibrium inertia tensor that governs the rotational stability.

## 3. Results

The non-equilibrium theory described above provides a generalized framework for assessing the rotational stability of a planet on the basis of its gravitational figure or, equivalently, its inertia tensor. In this section we reassess two issues that were previously investigated by applying a non-hydrostatic rotation theory to the figure of Mars. First, how stable is the present-day rotation vector of the planet? Second, what level of TPW was driven by the development of the Tharsis volcanic province?

### 3.1. The present-day rotational stability of Mars

We can write the total inertia tensor of Mars as

$$\begin{bmatrix} a \\ b \\ c \end{bmatrix} = \begin{bmatrix} \delta^{hyd}a \\ \delta^{hyd}b \\ \delta^{hyd}c \end{bmatrix} + \begin{bmatrix} \delta^{nhyd}a \\ \delta^{nhyd}b \\ \delta^{nhyd}c \end{bmatrix}, \tag{1}$$

where $a$, $b$, and $c$ are the non-dimensional moments (non-dimensionalized by the mass and mean radius of Mars) in the principal axis system ($a < b < c$) and the superscripts *hyd* and *nhyd* denote hydrostatic and non-hydrostatic contributions. On Mars, these three moments refer to axes on the equator at the same longitude as Tharsis, on the equator 90° from Tharsis, and the current rotation axis, respectively. Embedded within the hydrostatic component of the total inertia tensor is a spherical term which results in a trace, for this contribution, that is non-zero.

The non-hydrostatic moment increments are commonly expressed in terms of the observed harmonic (Stokes) coefficients of the gravitational potential at degree two, $J_2$ and $J_{22}$, in the same principal axis system (Bills and James, 1999):

$$\begin{bmatrix} \delta^{nhyd}a \\ \delta^{nhyd}b \\ \delta^{nhyd}c \end{bmatrix} = \begin{bmatrix} -1/3 \\ -1/3 \\ 2/3 \end{bmatrix} \left(J_2 - J_2^{hyd}\right) + \begin{bmatrix} -2 \\ 2 \\ 0 \end{bmatrix} J_{22}, \tag{2}$$

where the parameter $J_2^{hyd}$ is a correction to the observed $J_2$ harmonic associated with the hydrostatic form of the planet. Satellite-based measurements (Smith et al., 1999) have yielded the estimates: $J_2 = (1.960 \pm 0.02) \times 10^{-3}$ and $J_{22} = (6.317 \pm 0.003) \times 10^{-5}$.

This decomposition makes no assumption regarding a connection between the rotational stability and the inertia tensor. However, let us proceed by assuming that the non-hydrostatic

inertia tensor governs the rotational stability. In this case, once the observed harmonics $J_2$ and $J_{22}$ are specified, assessing the rotational stability reduces to estimating $J_2^{hyd}$ in Eq. (2). Bills and James (1999) combined a satellite-based estimate of $J_2$ with a constraint on the spin-axis precession rate (or precession constant) based on radio tracking from the Pathfinder mission (Folkner et al., 1997), to estimate the non-dimensional polar moment of inertia as $c = 0.3662 \pm 0.0017$. They then used the Darwin–Radau relationship to convert this value to an estimate for $J_2^{hyd} = 1.840 \pm 0.021 \times 10^{-3}$ [see their Eq. (88)]. Using this value in Eq. (2) yields:

$$\begin{bmatrix} \delta^{nhyd}a \\ \delta^{nhyd}b \\ \delta^{nhyd}c \end{bmatrix} = \begin{bmatrix} -166.06 \pm 7.20 \\ 86.63 \pm 7.20 \\ 79.43 \pm 14.27 \end{bmatrix} \times 10^{-6}. \tag{3}$$

Bills and James (1999) concluded, since $\delta^{nhyd}b > \delta^{nhyd}c$, that the current rotation pole of Mars is 90° from where it should be on the basis of the non-hydrostatic stability theory of Gold (1955). Moreover, since $\delta^{nhyd}b \sim \delta^{nhyd}c$, they also concluded that the pole is unstable; small mass loads would be capable of moving the pole along a great circle joining the maximum and intermediate axes of inertia (i.e., along the great circle 90° from Tharsis).

Yoder et al. (2003) have derived a more recent estimate of $c = 0.3650 \pm 0.0012$. We have repeated the Bills and James (1999) analysis for this range of values and the result is shown in Fig. 2. [One difference in our analysis is that we correct the polar moment $c$ for a small non-hydrostatic contribution before we apply the Darwin–Radau relation. Under the assumption that these non-hydrostatic contributions to the inertia tensor are axisymmetric about a point on the equator at the same longitude as Tharsis, the correction is simply $4J_{22}/3$ (Bills and James, 1999).] Over this entire range of $c$ values $\delta^{nhyd}b \sim \delta^{nhyd}c$, and therefore one would again conclude on the basis of a non-hydrostatic theory that the martian rotation pole is unstable. Note that the $c$ value adopted by Bills and James (1999) falls at the high end of the range considered in Fig. 2, and that $\delta^{nhyd}c > \delta^{nhyd}b$ when $c < 0.3657$.

As we noted in the last section, this non-hydrostatic theory is not appropriate for the analysis of Mars' rotational stability if the martian lithosphere is characterized by non-zero elastic strength. Accordingly, we need to analyze the non-equilibrium, rather than non-hydrostatic form to properly assess the stability. Simply put, the hydrostatic correction removes too much flattening from the observed form and will thus imply a significantly less stable planet than the correct, non-equilibrium approach.

Let us begin by re-writing Eq. (1) in the form:

$$\begin{bmatrix} a \\ b \\ c \end{bmatrix} = \begin{bmatrix} \delta^{eq}a \\ \delta^{eq}b \\ \delta^{eq}c \end{bmatrix} + \begin{bmatrix} \delta^{ne}a \\ \delta^{ne}b \\ \delta^{ne}c \end{bmatrix}, \tag{4}$$

where the superscripts *eq* and *ne* denote the equilibrium and non-equilibrium contributions to the total inertia tensor. The second of these contributions can be written in terms of $J_2$

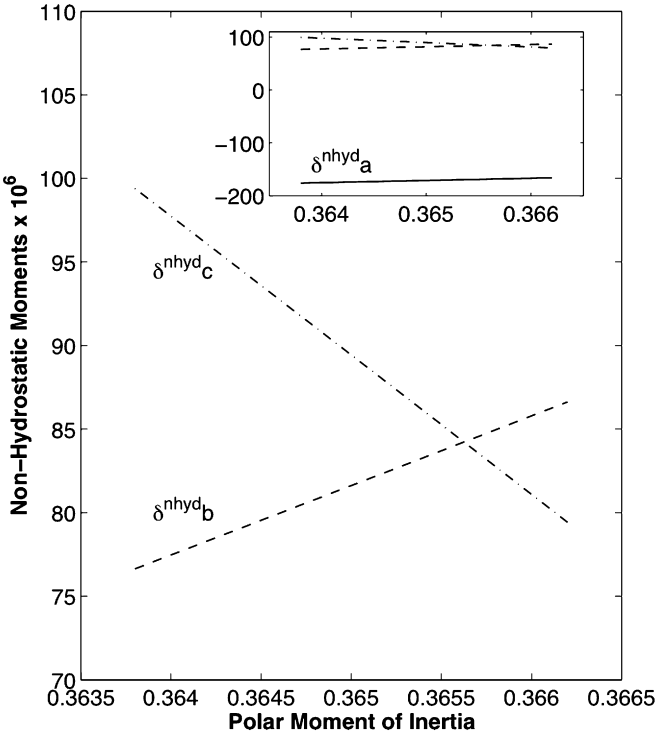


Fig. 2. Non-hydrostatic moments of inertia, computed using Eq. (2), as a function of the total polar moment of inertia, where the latter is varied within the uncertainty ($0.3650 \pm 0.0012$) cited by Yoder et al. (2003). The moments $\delta^{nhyd}c$ and $\delta^{nhyd}a$ refer to axes in the direction of the current rotation pole and the equatorial location of Tharsis. The axis associated with the moment $\delta^{nhyd}b$ is aligned with a point on the equator 90° from Tharsis. All moments are normalized by $Ma^2$, where $M$ and $a$ are the mass and mean radius of Mars. We adopt the observed values of $J_2 = 1.960 \times 10^{-3}$ and $J_{22} = 6.317 \times 10^{-5}$ cited in the main text.

and $J_{22}$ using a modified form of Eq. (2):

$$\begin{bmatrix} \delta^{ne}a \\ \delta^{ne}b \\ \delta^{ne}c \end{bmatrix} = \begin{bmatrix} -1/3 \\ -1/3 \\ 2/3 \end{bmatrix} \left(J_2 - J_2^{hyd}\right) + \begin{bmatrix} -1/3 \\ -1/3 \\ 2/3 \end{bmatrix} \left(J_2^{hyd} - J_2^{eq}\right) + \begin{bmatrix} -2 \\ 2 \\ 0 \end{bmatrix} J_{22}. \tag{5}$$

The second term on the right-hand side of this equation is the difference between the hydrostatic and equilibrium contributions to the inertia tensor and it can be written in the form [Eq. (A.17)]:

$$J_2^{hyd} - J_2^{eq} = \frac{\Omega^2 a^3}{3GM}\left[k_f^{T,*} - k_f^T\right], \tag{6}$$

where $a$ and $M$ are the radius and mass of the planet, respectively, and $G$ is the gravitational constant. The quantity within square brackets represents the difference between fluid Love numbers computed for no lithosphere (i.e., the hydrostatic form) and a lithosphere of thickness $LT$ (the equilibrium form).

In Fig. 3 we use Eqs. (5) and (6) to compute the non-equilibrium moments $\delta^{ne}a$, $\delta^{ne}b$ and $\delta^{ne}c$, as a function of the elastic lithospheric thickness. The Love numbers were computed using the Mars model of Sohl and Spohn (1997) (see

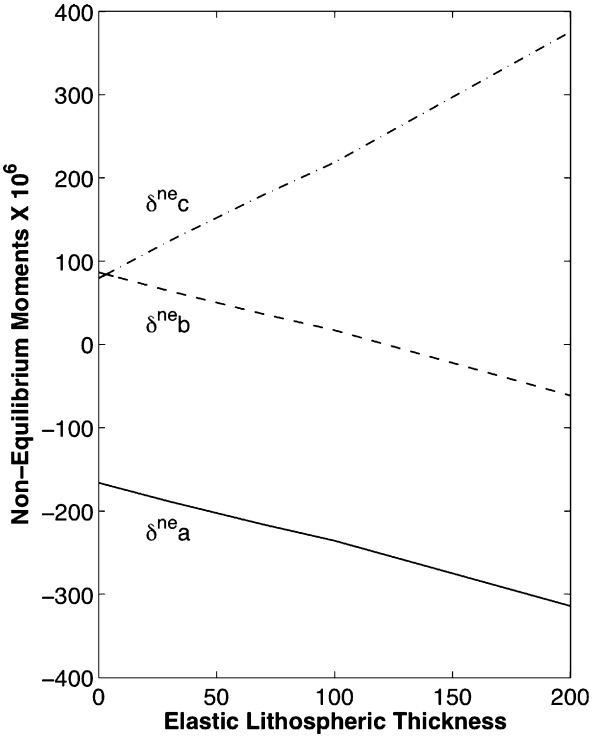


Fig. 3. Non-equilibrium moments of inertia, computed using Eqs. (5) and (6), as a function of the adopted thickness of the elastic lithosphere, $LT$ (km). The moments $\delta^{ne}a$, $\delta^{ne}c$, and $\delta^{ne}b$ refer to axes in the direction of Tharsis, the current rotation pole and a point on the equator 90° from Tharsis, respectively. All figures for the moments are normalized by $Ma^2$, where $M$ and $a$ are the mass and mean radius of Mars. We adopt the observed values of $J_2 = 1.960 \times 10^{-3}$ and $J_{22} = 6.317 \times 10^{-5}$ cited in the main text. The fluid Love numbers required in Eq. (6) are given in Table 1 for various values of $LT$.

Table 1
Effects of lithospheric thickness ($LT$) on the fluid $k$ Love numbers of Mars. We adopt the 5-layer model of martian structure described by Sohl and Spohn (1997). The tidal fluid Love number for $LT = 0$ is $k_f^{T,*} = 1.18955$

| $LT$ (km) | $k_f^L$ | $k_f^T$ |
|---|---|---|
| 30 | −0.951 | 1.146 |
| 70 | −0.910 | 1.091 |
| 100 | −0.875 | 1.053 |
| 200 | −0.764 | 0.899 |

Table 1). Furthermore, in evaluating the first term on the right-hand side of Eq. (5), we adopt the hydrostatic correction of Bills and James (1999). For $LT = 0$, the non-equilibrium theory collapses to the old non-hydrostatic case [$k_f^{T,*} = k_f^T$ in Eq. (6) and therefore the second term on the RHS of Eq. (5) vanishes] and the results suggest an unstable rotation pole (i.e., $\delta^{ne}b \sim \delta^{ne}c$, as noted in Fig. 2). However, the estimate of $\delta^{ne}c$ increases rapidly relative to $\delta^{ne}b$ as $LT$ is increased above zero. Indeed, a value of $LT = 100$ km yields a moment difference $\delta^{ne}c - \delta^{ne}b$ which is comparable to the difference $\delta^{ne}b - \delta^{ne}a$, and a highly stable rotation pole. We therefore conclude that the current orientation of the martian rotation pole is stable for values of $LT$ that are consistent with widely cited estimates (e.g., McGovern et al., 2004; Zhong and Roberts, 2003; Turcotte et al., 2002; Sohl and Spohn, 1997).

### 3.2. TPW driven by Tharsis loading

An important, outstanding issue in the long-term evolution of Mars concerns the extent to which the development of Tharsis changed the orientation of the rotation vector. For example, there have been numerous inferences of Tharsis-driven TPW based on tectonic patterns, geomorphologic features, magnetic anomalies and grazing impacts (see introduction and also Sprenke et al., 2005). In addition, there have been theoretical predictions of polar wander driven by a surface mass loading consistent with the size and current location of Tharsis (Melosh, 1980; Willemann, 1984; Matsuyama et al., 2006, 2007). These theoretical analyses admit both small and large polar wander solutions [TPW angle, $\delta$, of ∼10° or ∼80°, respectively; see discussion below Eq. (A.30)].

Sprenke et al. (2005) analyzed the observed figure of Mars using a non-hydrostatic stability theory and concluded that Tharsis induced a polar wander of 15°–90°. Specifically, they began by adopting the non-hydrostatic form given by Eq. (3) and then corrected this form for Tharsis using the load model of Zuber and Smith (1997). They next performed a search through all possible (pre-Tharsis) pole positions that satisfied the following stability equation (Bills and James, 1999):

$$J_2^{nhyd^\dagger} > 2J_{22}^{nhyd^\dagger}, \tag{7}$$

where the superscript † denotes the residual non-hydrostatic field after correction for Tharsis. The collection of acceptable pole positions defined a pre-Tharsis stability field, and the range of TPW angles that moved the pole from within this stability field to the present position yielded the inference of $\delta = 15°$–$90°$ (Sprenke et al., 2005).

To understand the origin of Eq. (7), we can consider a special case where the correction for Tharsis does not alter the principal axis orientation determined from the figure of Mars. In this case, we could revise Eq. (2) to remove the Tharsis load using:

$$\begin{bmatrix} \delta^{nhyd^\dagger}a \\ \delta^{nhyd^\dagger}b \\ \delta^{nhyd^\dagger}c \end{bmatrix} = \begin{bmatrix} -1/3 \\ -1/3 \\ 2/3 \end{bmatrix} \left(J_2 - J_2^{hyd} - J_2^\dagger\right) + \begin{bmatrix} -2 \\ 2 \\ 0 \end{bmatrix} \left(J_{22} - J_{22}^\dagger\right), \tag{8}$$

where $J_2^\dagger$ and $J_{22}^\dagger$ are the Tharsis contributions to these coefficients. If we define $J_2^{nhyd^\dagger} = J_2 - J_2^{hyd} - J_2^\dagger$ and $J_{22}^{nhyd^\dagger} = J_{22} - J_{22}^\dagger$, then the stability equation (7) is seen simply as a condition that $\delta^{nhyd^\dagger}c > \delta^{nhyd^\dagger}b$.

There are various assumptions inherent to the procedure adopted by Sprenke et al. (2005). First, that the non-hydrostatic form governs the rotational stability (see their discussion on p. 488). Second, related to the first, that the remnant bulge dynamics discussed by Willemann (1984) may be ignored. This assumption is implied by the procedure of searching through possible pre-Tharsis pole positions. In the physics of Fig. 1C, each reorientation of the pole in this manner would introduce a remnant bulge contribution to both the $J_2$ and $J_{22}$ that should

be accounted for. A further assumption of Sprenke et al. (2005) is that the figure of Mars at spherical harmonic degree two has not changed, with the exception of a simple rotation, subsequent to the end of the development of Tharsis [i.e., the values of $J_2$ and $J_{22}$ used in Eq. (7) are present-day values].

In this section, we revisit the inference of Tharsis-driven TPW based upon the observed figure of Mars by using the non-equilibrium rotation theory appropriate to the physics of Fig. 1C. In Appendix A.2 we derive expressions for the total Stokes coefficients $J_2$ and $J_{22}$ (in the principal axis system) arising from the loading of a planet within this scenario [Eqs. (A.31) and (A.32)]. For the benefit of the reader, we repeat these equations here:

$$J_2 = k_f^T \frac{\Omega^2 a^3}{3GM} + \left(1 + k_f^L\right) k_f^{T,*} Q' \frac{\Omega^2 a^3}{3GM} \left[\frac{1 - 3\cos^2\theta_L}{2}\right] - \left(k_f^{T,*} - k_f^T\right) \frac{\Omega^2 a^3}{3GM} \left[\frac{1 - 3\cos^2\delta}{2}\right],$$

$$4J_{22} = \left(1 + k_f^L\right) k_f^{T,*} Q' \frac{\Omega^2 a^3}{3GM} \sin^2\theta_L - \left(k_f^{T,*} - k_f^T\right) \frac{\Omega^2 a^3}{3GM} \sin^2\delta,$$

where the TPW angle $\delta$ is given by [Eq. (A.29)]:

$$\delta = \frac{1}{2} \arcsin\left[Q'\alpha \sin(2\theta_L)\right]$$

and $\alpha$ is a parameter which depends on the planetary model and the adopted lithospheric thickness [Eq. (A.30)]:

$$\alpha = \frac{1 + k_f^L}{1 - k_f^T / k_f^{T,*}}.$$

These expressions yield the Stokes coefficients for the final state given by Fig. 1C4. In these equations, $\theta_L$ denotes the final colatitude of the Tharsis load, which we take to be 83° (Zuber and Smith, 1997). For a given model of Mars' density structure, which yields $k_f^{T,*}$ (Table 1), there are two free parameters on the RHS of these equations. The first is the lithospheric thickness. Specifying $LT$ sets the values of the fluid tide and load Love numbers, $k_f^T$ and $k_f^L$, respectively (Table 1), as well as the parameter $\alpha$. The second is the uncompensated size of the Tharsis load, $Q'$ [Eq. (A.26)], defined as the ratio of the gravitational potential perturbation at degree 2 due to the direct effect of the load and the hydrostatic bulge [the latter, together with $LT$, sets the angle $\delta$ in Eq. (A.29)].

Our procedure for determining the range of acceptable TPW angles $\delta$ driven by the Tharsis load is as follows. First, we specify some tolerance within which the predictions should fit the observed values of the Stokes coefficients $J_2$ and $J_{22}$. Next, we choose a value of $LT$. For this lithospheric thickness, we then search through a wide range of $Q'$ values and note all predictions that fit the Stokes coefficients. We then repeat this procedure for different choices of $LT$. For each $Q'$, this provides a range of acceptable $\delta$ values (this range can be zero).

Equations (A.31) and (A.32) assume that the only contributors to the non-equilibrium planetary form are the Tharsis load (represented by $Q'$) and the remnant bulge (whose contribution depends on the level of TPW). Although Tharsis dominates the observed gravitational form of Mars, not including other loading contributions and their associated TPW will introduce some error in our predictions of both $J_2$ and $J_{22}$, and the misfit tolerance we discuss above is an attempt to explore the sensitivity of our inferences to this error.

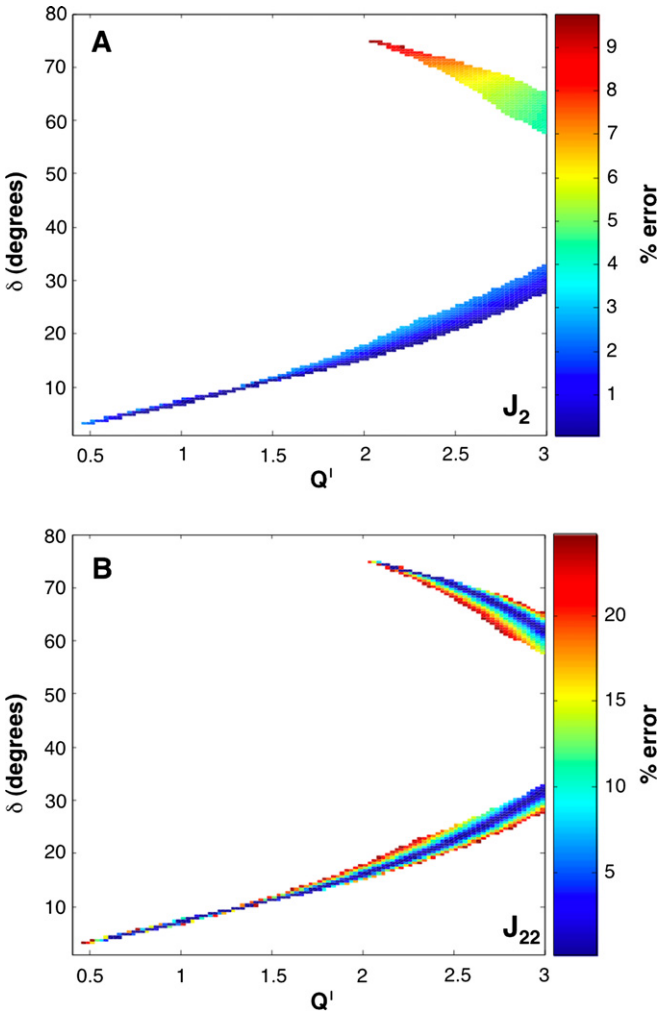


Fig. 4. The full range of TPW angles, $\delta$, as a function of the uncompensated size of Tharsis, $Q'$, that yield 'acceptable' fits to the observed Stokes coefficients $J_2$ and $J_{22}$ for the present-day gravitational figure of Mars. The calculations are based on the non-equilibrium stability theory summarized in Fig. 1C and by Eqs. (A.29)–(A.32). These predictions adopt a final Tharsis colatitude of 83° (Zuber and Smith, 1997), and a lithospheric thickness, $LT$, which varies from 30 to 200 km. The range of solutions includes all predictions which fit the observed $J_2$ and $J_{22}$ coefficients to within 10 and 25%, respectively. The color contours in (A) show the variation in the $J_2$ misfit across the range of acceptable solutions. (B) is the analogous result for the $J_{22}$ misfit.

In Fig. 4 we show all acceptable solutions for $\delta$ as a function of the uncompensated size of the load when we allow a misfit of up to 10% of the observed value of $J_2$ and up to 25% of the value of $J_{22}$. [These different values reflect the fact that the background rotational bulge dominates the $J_2$ observation; as an example, the non-hydrostatic figure of Mars inferred by Bills and James (1999) is ~6% of the observed value.] Fig. 4A maps out the variation in the misfit to the $J_2$ coefficient (as indi-

cated by the color bar) within the range of acceptable solutions, while Fig. 4B is the analogous map for the $J_{22}$ harmonic. Embedded within these calculations are elastic lithospheric thicknesses ranging from 30 to 200 km.

No solutions exist below a $Q'$ value of 0.45. Moreover, in our calculations we adopt an upper bound $Q'$ value of 3.0, which is significantly larger than the bound cited by Willemann (1984). As discussed in Appendix A.2, there are, in theory, two possible true polar wander solutions for a given load size and final colatitude when $Q'\alpha > 1$; in this case, if $\delta$ is a solution of Eq. (A.29), then $90° - \delta$ is also a solution. However, both solutions are not necessarily able to reconcile the additional constraint we have imposed in regard to the fit to the observed Stokes coefficients. For example, high TPW solutions (i.e., greater than 45°) do exist, but only for $Q' > 2$ and a mismatch to the observed value of $J_2 > 4\%$ (for $Q' < 3$). As we allow a progressively greater mismatch to the $J_2$ coefficient, high TPW solutions are found for progressively lower values of $Q'$.

A comparison of Figs. 4A and 4B indicates that the $J_2$ coefficient provides a more stringent constraint on the acceptable range of TPW than $J_{22}$. As an example, while high TPW solutions only exist for a misfit tolerance greater than 4% of $J_2$, these solutions span a wide range of $J_{22}$ misfits (i.e., from less than a percent upwards). We conclude, under the assumptions inherent to the present analysis, that the development of Tharsis could only have driven a large excursion of the pole if a significant fraction of the present-day $J_2$ observation is due to signals from sources other than Tharsis and its associated remnant bulge reorientation. The size of this required contribution, which reaches ~10% for $Q' = 1.7$ (Willemann, 1984), is larger than any surface load found on Mars (Smith et al., 1999). This suggests that the only plausible source would be related to internal, convectively-driven dynamics. We can rephrase this by concluding that the $J_2$ signal associated with a large TPW event (and remnant bulge reorientation) driven by Tharsis differs significantly from the present-day observation of this harmonic.

The relationship between the lithospheric thickness and misfit within the suite of acceptable TPW solutions shown in Fig. 4 is plotted in Fig. 5. That is, for a given $Q'$, Fig. 5 provides the range in $LT$ embedded within the solutions for $\delta$ on the associated frame of Fig. 4. Note that for both the low and high TPW solutions, the elastic thickness of the lithosphere which produced a solution for the Stokes coefficients within the specified misfit tolerances tends to decrease as $Q'$ is increased.

This trend reveals some interesting physics. Consider, first, the small TPW branch of solutions. The results in Fig. 4 indicate that a small Tharsis load ($Q' \sim 0.5$) emplaced at a colatitude very close to its final colatitude (i.e., $\delta$ of a few degrees) will yield a good fit to both the $J_2$ and $J_{22}$ observations. Increasing the uncompensated size of the load will increase the TPW angle $\delta$ (Fig. 4). To maintain a similar fit to the gravitational field as $Q'$ is increased, that is, to maintain a similar effective load size and remnant bulge signal, requires, in this case, that the lithospheric thickness be reduced. Next, within the high TPW branch, decreasing $Q'$ leads to a higher, not smaller, level of TPW (Fig. 4). Once again, one can maintain a similar contribution to the Stokes coefficients from the surface load by

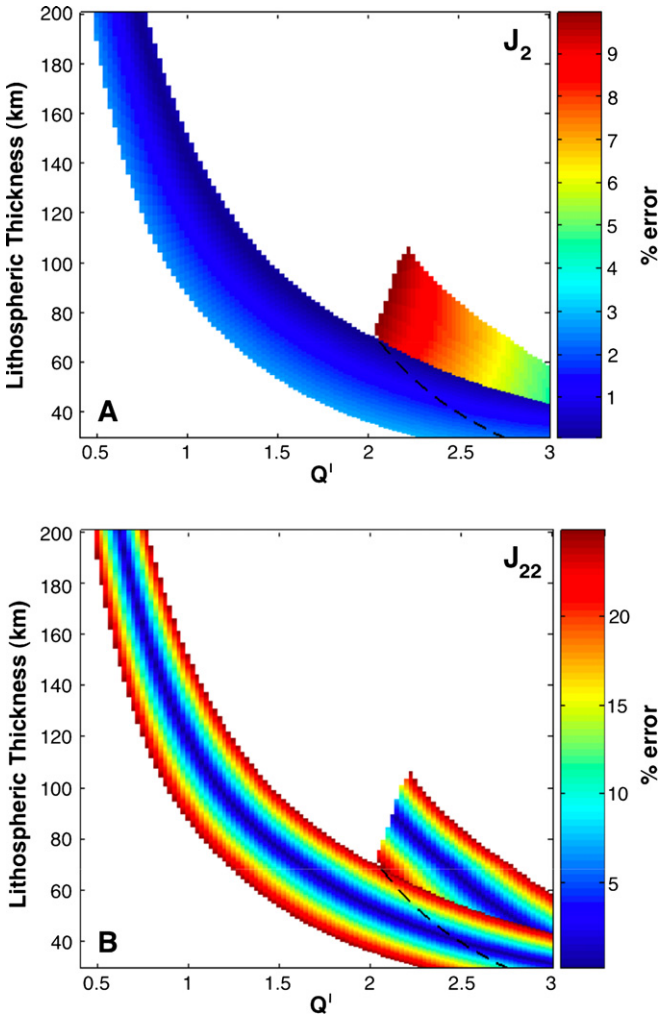


Fig. 5. The range of lithospheric thickness, as a function of the uncompensated size of Tharsis, that yield 'acceptable' fits to the observed Stokes coefficients $J_2$ and $J_{22}$ for the gravitational figure of Mars. The associated range in TPW angles, $\delta$, is given in Fig. 4. The details of the calculation are discussed in the caption to Fig. 4 and in the text. (A) and (B) show the variation in the $J_2$ and $J_{22}$ misfit across this range of acceptable solutions.

increasing $LT$ as $Q'$ is decreased since this will reduce the level of isostatic compensation. However, in this case, the signal from remnant bulge reorientation will not remain the same; rather it will increase because both the TPW angle and the size of the remnant bulge will increase. The result is an increasing level of $J_2$ misfit as $Q'$ is decreased in the high TPW branch.

Under the assumptions inherent to the analysis, Figs. 4 and 5 may be used to constrain the thickness of the martian lithosphere at the time of the formation of Tharsis and the TPW driven by this formation. As discussed above, if we accept an upper bound on the (uncompensated) size of Tharsis cited by Willemann (1984), $Q' = 1.7$, then high TPW solutions are ruled out unless the misfit to $J_2$ is well over 10%. In this particular case, the TPW angle is limited to less than 15° (Willemann, 1984; Matsuyama et al., 2006) and the minimum elastic thickness of the martian lithosphere at Tharsis formation would be 45 km. For a $Q'$ value of 1, the TPW angle would be less than 10°, and $LT > 90$ km.

## 4. Conclusions

Numerous analyses of the rotational stability of Mars, either at present day or in response to loading by Tharsis, have been based on the assumption that this stability is governed by the non-hydrostatic gravitational figure of the planet. We have demonstrated that such a treatment is incorrect. In particular, for any planet with long-term elastic strength within the lithosphere, the stability of the rotation vector is governed by the gravitational figure after correction for an 'equilibrium,' rather than hydrostatic form. The former is defined as the shape achieved by an initially non-rotating planet with an elastic outer shell after all viscous stresses below the shell have relaxed subsequent to the onset of rotation (e.g., Fig. 1B1). The equilibrium form depends on the thickness of the elastic plate as well as on the rotation rate and the internal density structure of the planet, and it is the component of the gravitational figure which will perfectly reorient (in the fluid limit) to a change in the rotation vector; thus, it provides no long-term memory of any previous rotational state. The 'non-equilibrium' theory provides the necessary extension of the oft-cited non-hydrostatic theory of Gold (1955) to the case of planets with lithospheres that maintain elastic strength over very long time scales.

The observed figure of Mars, after correction for the equilibrium form, indicates that the present-day rotation axis of the planet is stable for adopted elastic thicknesses of the martian lithosphere well below current estimates (Fig. 3). This counters previous conclusions, based on a non-hydrostatic theory of planetary rotation, that the present-day orientation of the pole is unstable and will move easily on a great circle defined by the arc joining the current pole and a point 90° from Tharsis on the martian equator.

Finally, we have used a version of the non-equilibrium theory valid for the scenario of planetary evolution considered by Willemann (1984) and Matsuyama et al. (2006), in which a lithosphere develops on an initially hydrostatic form, to estimate the range of possible Tharsis-driven TPW. Our analysis, based on a comparison of predictions of the Stokes coefficients $J_2$ and $J_{22}$ with present-day observational constraints, suggests that Tharsis drove less than 15° of polar motion. These calculations also indicate that $LT$ at the time of Tharsis formation was at least ∼50 km, though a more likely lower bound (if we accept $Q' \sim 1$) is ∼100 km. This bound suggests that the formation of Tharsis did not markedly reduce the strength of the martian lithosphere.

This inference of Tharsis-driven TPW assumes that the figure of Mars has been altered by a relatively minor amount, defined by an imposed misfit tolerance, since the end of Tharsis formation. We can clearly not rule out that other loads, in particular internal heterogeneity related to convection, provide a significant contribution to the present-day form. However, our intent was to specifically reassess the conclusions of previous work that had assumed that these contributions were small. In this regard, our results demonstrate that arguments that Tharsis-induced TPW was at least 15°, based on a non-hydrostatic theory of martian rotational stability, are not robust.

## Acknowledgments

This work was supported by CIFAR, NSERC, NSF, the Carnegie Institution of Washington, a Daly Fellowship (to T.P.), the NASA Astrobiology Institute (NNA04CC02A) and the Miller Institute.

## Appendix A. Mathematical treatment of Fig. 1

In this appendix we use standard (fluid) Love number theory to derive expressions for the inertia tensor appropriate to each of the scenarios in Fig. 1. In each case, we consider the connection between these expressions and the $J_2$ and $J_{22}$ harmonics within the principal axis system. The reader is asked to note that prior to Eq. (A.29), the symbol $\delta$ refers to the Kronecker delta and not the TPW angle.

In the time domain ($t$), the viscoelastic load and tidal (or tidal-effective) $k$ Love numbers at spherical harmonic degree two have the form (Peltier, 1974):

$$k^L(t, LT) = k^{L,E}\delta(t) + \sum_{j=1}^{J} r_j \exp(-s_j t) \tag{A.1}$$

and

$$k^T(t, LT) = k^{T,E}\delta(t) + \sum_{j=1}^{J} r'_j \exp(-s_j t). \tag{A.2}$$

These Love numbers yield the gravitational potential perturbation, at degree two, arising from the deformation of a spherically symmetric, Maxwell viscoelastic planetary model subject to an impulsive surface mass load and gravitational potential (tidal) forcing, respectively. The first term on the right-hand side (henceforth RHS) of each expression represents the immediate elastic response to the loading (hence the superscript $E$), while the second term is a non-elastic response comprised of a series of $J$ normal modes of viscoelastic decay. The modes for the load and tidal Love numbers have a common set of decay times ($s_j$), but distinct modal amplitudes ($r_j$ and $r'_j$). These Love numbers are dependent on the viscoelastic structure of the planetary model. For our purposes the dependence on the elastic thickness of the lithosphere ($LT$) is most important, and thus we make this dependence explicit. In the Laplace transform domain, these Love numbers have the form:

$$k^L(s, LT) = k^{L,E} + \sum_{j=1}^{J} \frac{r_j}{s + s_j} \tag{A.3}$$

and

$$k^T(s, LT) = k^{T,E} + \sum_{j=1}^{J} \frac{r'_j}{s + s_j}. \tag{A.4}$$

The so-called fluid Love numbers represent the response of the planetary model after all viscous stresses have relaxed. These may be derived from the above expressions either by taking the $s = 0$ limit of the Laplace-domain equations (A.3) and (A.4), or by convolving the time-domain equations (A.1)

and (A.2) with a Heaviside step loading and considering the infinite time response. In either case, we would then obtain:

$$k_f^L(LT) = k^{L,E} + \sum_{j=1}^{J} \frac{r_j}{s_j} \tag{A.5}$$

and

$$k_f^T(LT) = k^{T,E} + \sum_{j=1}^{J} \frac{r'_j}{s_j}. \tag{A.6}$$

The fluid Love numbers are dependent on the density profile of the planetary model, as well as the thickness of the elastic lithosphere. The latter is, of course, subject to no viscous relaxation. For the sake of brevity, we will suppress the dependence on $LT$ in equations that require the fluid Love numbers (e.g., $k_f^L$, $k_f^T$). However, in the case of a purely hydrostatic planet, i.e., one which has no long-term elastic strength ($LT = 0$), we will adopt the notation $k_f^{L,*}$ and $k_f^{T,*}$.

### *A.1. The inertia tensor: Three case studies*

We assume a co-ordinate system oriented so that the $z$-axis is fixed to the rotation pole of the planet just prior to loading (e.g., Figs. 1A1, 1B1, or 1C1). The initial angular velocity vector will be denoted by $(0, 0, \Omega)$. At any subsequent time, the rotation vector will be given by $\omega_i(t), i = 1, 2, 3$, with magnitude $\omega^2(t)$. Finally, $a$ and $M$ are the radius and mass of the planet, respectively, while $G$ is the gravitational constant.

#### *A.1.1. Case 1: Gold (1955)*

We begin with the scenario in Fig. 1A, which is the physics treated by Gold (1955). In this case, the total inertia tensor is (Munk and MacDonald, 1960; Ricard et al., 1993):

$$I_{ij}(t) = I_0\delta_{ij} + \frac{a^5 k_f^{T,*}}{3G}\left[\omega_i(t)\omega_j(t) - \frac{1}{3}\omega^2(t)\delta_{ij}\right] + I_{ij}^L(t), \tag{A.7}$$

where $I_0$ is the spherical term and $I_{ij}^L(t)$ is the contribution to the inertia tensor from the combined effect of the surface mass load and the direct planetary deformation it induces. The second term on the right-hand side is related to the rotationally-induced flattening of the hydrostatic model adopted by Gold (1955).

The first two terms on the RHS constitute the inertia tensor for a hydrostatic planet with angular velocity $\omega_i(t)$. Thus, we can write

$$I_{ij}^{hyd}(t) = I_0\delta_{ij} + \frac{a^5 k_f^{T,*}}{3G}\left[\omega_i(t)\omega_j(t) - \frac{1}{3}\omega^2(t)\delta_{ij}\right]. \tag{A.8}$$

This represents the component of the inertia tensor in Eq. (A.7) that perfectly adjusts (in the fluid limit) to any change in the rotation axis (i.e., as in the fully relaxed cases shown in Figs. 1A1, 1A3, and 1A4). As discussed by Gold (1955), this component is not relevant to the long-term rotational stability of the (hydrostatic) planet since it provides no memory of any previous orientation of the rotation vector. Thus, for this planetary model, the reorientation of the pole is governed by the non-hydrostatic inertia tensor:

$$I_{ij}^{nhyd}(t) = I_{ij}^L(t). \tag{A.9}$$

In particular, the rotation vector is aligned with the maximum principal axis of $I_{ij}^{nhyd}$. Thus, the adjustment in Fig. 1A will continue until the load has moved to the equator (Fig. 1A4).

It will be instructive to consider the inertia tensor in the initial ($t = t_0$), unloaded state of the system. Applying the initial rotation vector, $(0, 0, \Omega)$, into the expression $[\omega_i(t)\omega_j(t) - \frac{1}{3}\omega^2(t)\delta_{ij}]$ within Eq. (A.8) yields:

$$I_{ij}^{hyd}(t_0) = I_0\delta_{ij} + \frac{\Omega^2 a^5 k_f^{T,*}}{3G}\left(\delta_{i3} - \frac{1}{3}\right)\delta_{ij}. \tag{A.10}$$

The orientation in Fig. 1A1 is a principal axis orientation, and thus we may use this expression to derive a formula for the hydrostatic component of the $J_2$ harmonic (Bills and James, 1999):

$$J_2^{hyd} = \frac{I_{33}^{hyd} - \frac{I_{11}^{hyd} + I_{22}^{hyd}}{2}}{Ma^2} = \frac{\Omega^2 a^3 k_f^{T,*}}{3GM}. \tag{A.11}$$

As a final point we note an inherent inconsistency in the Gold (1955) scenario. In a purely hydrostatic planet, the contribution to the inertia tensor from the load and direct deformation, $I_{ij}^L$, will be zero, since the load will be perfectly isostatically compensated. In the terminology of fluid Love number theory, the uncompensated fraction of an applied load is given by $1 + k_f^L$, but as $LT$ approaches zero $k_f^L \to k_f^{L,*} = -1$. Thus, the scenario in Fig. 1A only holds if one makes the ad-hoc assumption that the rotational bulge will be perfectly relaxed in the fluid limit, but that the load will not be perfectly compensated.

#### *A.1.2. Case 2: The equilibrium form*

Next, we turn to the scenario in Fig. 1B. The relevant expression for the total inertia tensor is trivially derived from Eq. (A.7) by replacing the hydrostatic ($LT = 0$) fluid tidal Love number with the more general case $k_f^T$. This yields

$$I_{ij}(t) = I_0\delta_{ij} + \frac{a^5 k_f^T}{3G}\left[\omega_i(t)\omega_j(t) - \frac{1}{3}\omega^2(t)\delta_{ij}\right] + I_{ij}^L(t). \tag{A.12}$$

In this case, the component of the inertia tensor that perfectly reorients to a change in the rotation vector (as in Figs. 1B1, 1B3, and 1B4) is given by the first two terms on the right-hand side of Eq. (A.12). These terms represent the equilibrium (i.e., relaxed) form achieved by a rotating planet with an elastic shell (Mound et al., 2003). We will denote this equilibrium form as

$$I_{ij}^{eq}(t) = I_0\delta_{ij} + \frac{a^5 k_f^T}{3G}\left[\omega_i(t)\omega_j(t) - \frac{1}{3}\omega^2(t)\delta_{ij}\right]. \tag{A.13}$$

Once again, this component of the total inertia tensor does not play a role in the long-term rotational stability of the planet since it provides no memory of any previous rotational state. Therefore, the reorientation of such a planet is governed by the

non-equilibrium component of the inertia tensor:

$$I_{ij}^{neq}(t) = I_{ij}^{L}(t). \tag{A.14}$$

As in the first scenario (Fig. 1A), the pole will be aligned with the maximum principal axis of $I_{ij}^{L}(t)$, and thus the load will ultimately move to a position on the equator (Fig. 1B4). However, in contrast to the scenario in Fig. 1A, we need not make an ad-hoc assumption that the load will never be perfectly compensated. This incomplete compensation is assured by the presence of the elastic lithosphere, and in this sense the scenario in Fig. 1B is a more self-consistent illustration of the physics that Gold (1955) was highlighting.

In analogy to the first case, an expression for the equilibrium inertia tensor in the initial configuration of Fig. 1B1 is

$$I_{ij}^{eq}(t_0) = I_0\delta_{ij} + \frac{\Omega^2 a^5 k_f^T}{3G}\left(\delta_{i3} - \frac{1}{3}\right)\delta_{ij} \tag{A.15}$$

and thus the equilibrium component of the $J_2$ harmonic is given by

$$J_2^{eq} = \frac{I_{33}^{eq} - \frac{I_{11}^{eq}+I_{22}^{eq}}{2}}{Ma^2} = \frac{\Omega^2 a^3 k_f^T}{3GM}. \tag{A.16}$$

We can derive an expression for the difference between the hydrostatic and equilibrium components of the $J_2$ harmonic. This is obtained by subtracting Eq. (A.16) from (A.11):

$$J_2^{hyd} - J_2^{eq} = \frac{\Omega^2 a^3}{3GM}\left[k_f^{T,*} - k_f^T\right]. \tag{A.17}$$

This is identical to Eq. (6) within the main text.

### *A.1.3. Case 3: A remnant rotational bulge*

The rotating form of a planet will be established early in its history, prior to the development of an elastic lithosphere. Accordingly, Willemann (1984) suggested that the rotational stability of a planet with a lithosphere will be governed by the physics summarized in Fig. 1C. The scenario assumes that the initial rotating form will be hydrostatic (Fig. 1C0); the subsequent development of the lithosphere through cooling of the planet will not alter this hydrostatic form (Fig. 1C1) since no elastic stresses will be introduced within the plate. However, any subsequent surface mass loading and perturbation to the centrifugal potential (Fig. 1C2 onwards) *will* introduce such stresses within the lithosphere. Thus, the planetary model that governs the response to such loads ($LT \neq 0$) will be different from the model that governs the initial form ($LT = 0$).

In this case, the total inertia tensor of the planet subsequent to the application of the surface load is

$$\begin{aligned} I_{ij}(t) = {} & I_0\delta_{ij} + \frac{\Omega^2 a^5 k_f^{T,*}}{3G}\left(\delta_{i3} - \frac{1}{3}\right)\delta_{ij} \\ & + \frac{a^5 k_f^T}{3G}\left\{\left[\omega_i(t)\omega_j(t) - \frac{1}{3}\omega^2(t)\delta_{ij}\right] \right. \\ & \left. - \Omega^2\left(\delta_{i3} - \frac{1}{3}\right)\delta_{ij}\right\} + I_{ij}^{L}(t). \end{aligned} \tag{A.18}$$

The first two terms on the RHS represent the original hydrostatic form of the planet [Fig. 1C1; compare this equation with Eq. (A.10) and note that this form is identical to that in Fig. 1A1]. The third term is the contribution from the response of the planet (with $LT \neq 0$) to the perturbed centrifugal potential.

We can re-arrange Eq. (A.18) into the following form

$$\begin{aligned} I_{ij}(t) = {} & I_0\delta_{ij} + \frac{a^5 k_f^T}{3G}\left[\omega_i(t)\omega_j(t) - \frac{1}{3}\omega^2(t)\delta_{ij}\right] \\ & + \frac{\Omega^2 a^5}{3G}\left(\delta_{i3} - \frac{1}{3}\right)\delta_{ij}\left[k_f^{T,*} - k_f^T\right] + I_{ij}^{L}(t). \end{aligned} \tag{A.19}$$

As discussed above, any term in the inertia tensor that perfectly adjusts to a change in the rotation vector will provide no memory of a previous rotational state and will thus have no bearing on the long-term stability of the rotation pole. In this regard, the form of Eq. (A.19) allows a natural separation between terms which adjust perfectly (first and second terms on the RHS) and those that do not (third and fourth terms). The former is simply

$$I_{ij}^{eq}(t) = I_0\delta_{ij} + \frac{a^5 k_f^T}{3G}\left[\omega_i(t)\omega_j(t) - \frac{1}{3}\omega^2(t)\delta_{ij}\right] \tag{A.20}$$

which is identical to the equilibrium form defined in Eq. (A.13). That is, in the scenario of Fig. 1C, the component of the inertia tensor that adjusts perfectly (in the fluid limit) to the change in pole position is the same as it was in Fig. 1B—namely, the equilibrium form for a rotating planet with an elastic shell (Fig. 1B1). Thus the rotational stability is once again governed by the non-equilibrium inertia tensor. From Eqs. (A.19) and (A.20), this term is given by

$$I_{ij}^{neq}(t) = \frac{\Omega^2 a^5}{3G}\left(\delta_{i3} - \frac{1}{3}\right)\delta_{ij}\left[k_f^{T,*} - k_f^T\right] + I_{ij}^{L}(t). \tag{A.21}$$

The first term on the right-hand side of this equation is aligned with the initial form of the planet (i.e., the orientation at the time of the development of the lithosphere) and it is known as the remnant rotational bulge (Willemann, 1984; Matsuyama et al., 2006). The long-term reorientation of the pole is thus governed by a balance between this term, which acts to resist (and thus stabilize) the motion of the pole, and the loading term, which acts to push the pole away. The result is a final load position that lies less than 90° from the pole (Fig. 1C4).

In the scenario of Fig. 1C, the determination of the long-term TPW reduces to a diagonalization of the non-equilibrium inertia tensor given by Eq. (A.21). This is the procedure followed by both Willemann (1984) and Matsuyama et al. (2006), though they did not explicitly identify their expressions as representing non-equilibrium forms. Indeed, Matsuyama et al. (2006) referred to a diagonalization of the non-hydrostatic form, where 'hydrostatic' was intended to mean the form in which all viscous relaxation in the region below the elastic lithospheric region was complete. We prefer here to use the term non-equilibrium for the $LT \neq 0$ case in order to avoid confusion with the hydrostatic ($LT = 0$) terminology inherent to Case 1 (Fig. 1A).

We can use the equilibrium inertia tensor to derive an expression for the equilibrium $J_2$ harmonic. As in Case 2, this expression is

$$J_2^{eq} = \frac{I_{33}^{eq} - \frac{I_{11}^{eq}+I_{22}^{eq}}{2}}{Ma^2} = \frac{\Omega^2 a^3 k_f^T}{3GM}. \tag{A.22}$$

### A.2. Stokes coefficients for Case 3: Axisymmetric loading

Within the main text we use the remnant bulge scenario to explore the range of pre-Tharsis orientations that yield a total inertia tensor consistent with observational constraints on the $J_2$ and $J_{22}$ harmonics. In this section, we derive expressions for the total (principal axis system) $J_2$ and $J_{22}$ harmonics arising from the Case 3 scenario. For this purpose, following Zuber and Smith (1997), we model Tharsis as an axisymmetric load.

We begin by defining an arbitrary spherical harmonic decomposition (degree $\ell$, order $m$) of a scalar field $\Lambda$ as

$$\Lambda(\theta,\phi) = \sum_{\ell=0}^{\infty}\sum_{m=-\ell}^{\ell} \Lambda_{\ell,m} Y_{\ell,m}(\theta,\phi), \tag{A.23}$$

where $\theta$ and $\phi$ are the colatitude and east-longitude, respectively, and the $Y_{\ell,m}$ are surface spherical harmonics normalized such that

$$\int_S Y^{\dagger}_{\ell',m'}(\theta,\phi) Y_{\ell,m}(\theta,\phi)\,\mathrm{d}S = 4\pi\delta_{\ell\ell'}\delta_{mm'}. \tag{A.24}$$

The symbol † denotes the complex conjugate and $S$ is the complete solid angle.

Let us assume that the axisymmetric surface mass load, if placed at the north pole, is characterized by a degree-two spherical harmonic coefficient of $L'_{2,0}$. If this load is placed at an arbitrary position $(\theta_L, \phi_L)$, then one can show that the harmonic coefficients at degree two for this load orientation are given by

$$L_{2,m} = \frac{L'_{2,0}}{\sqrt{5}} Y^{\dagger}_{2,m}(\theta_L,\phi_L). \tag{A.25}$$

It will be convenient, following Willemann (1984) and Matsuyama et al. (2006), to represent the size of the load by the ratio of the degree two gravitational potential perturbation due to the direct effect of the load and the hydrostatic rotational bulge. If we use the symbol $Q'$ to denote this ratio, then (Matsuyama et al., 2006)

$$Q' = -\frac{\frac{4\pi a^3 g}{5M} L'_{2,0}(t)}{\frac{-1}{3\sqrt{5}} a^2\Omega^2 k_f^{T,*}}, \tag{A.26}$$

where $g$ is the surface gravitational acceleration.

The degree two components of the load, as represented in Eqs. (A.25) and (A.26), may be converted into inertia tensor perturbations $I_{ij}^L(t)$ using the following mapping (Matsuyama et al., 2007):

$$I_{ij}^L = Q'\big(1+k_f^L\big)k_f^{T,*}\frac{\Omega^2 a^5}{3G}\left[\frac{1}{3}\delta_{ij} - e_i^L e_j^L\right]. \tag{A.27}$$

Here, $e_i^L$ is a unit vector in the direction of the load and is equal to

$$e_i^L = (\sin\theta_L\cos\phi_L, \sin\theta_L\sin\phi_L, \cos\theta_L). \tag{A.28}$$

This expression for the load inertia tensor is written in terms of the final colatitude of the load (i.e., the colatitude in a reference frame in which the $z$-axis is aligned with the rotation pole). This form of (A.27) can then be substituted into an analogously modified version of our equation for the non-equilibrium inertia tensor (A.21). Diagonalizing the result yields the following expression for the TPW angle $\delta$ (Matsuyama et al., 2006)

$$\delta = \frac{1}{2}\arcsin\big[Q'\alpha\sin(2\theta_L)\big]. \tag{A.29}$$

Here, $\alpha$ is a parameter dependent on the planetary model (and, in particular, $LT$):

$$\alpha = \frac{1+k_f^L}{1-k_f^T/k_f^{T,*}}. \tag{A.30}$$

As a consequence of the symmetry of the load, the reorientation of the pole occurs along the great circle that includes the load longitude, $\phi_L$. The sign convention is such that $\delta$ is the angle directed away from the load when $Q' > 0$ (as implied by Fig. 1C).

The solution in Eq. (A.29) is an extension of the expression derived by Willemann (1984), who applied approximations that led him to conclude that the TPW angle was independent of the lithospheric thickness (i.e., $\alpha = 1$ in this earlier study). If we define $Q_{eff} = Q'\alpha$, then when $Q_{eff} \leqslant 1$ there is one admissible solution for a given value of the final load colatitude; in contrast, there are two solutions, $\delta$ and $90-\delta$, when $Q_{eff} > 1$ (Matsuyama et al., 2006, Fig. 2). As an example, Willemann (1984) estimated an upper bound value of $Q' = 1.74$. Using this value in Eq. (A.29), and the fluid Love numbers in Table 1, yields solutions of $\delta \sim 10°$ or $\sim 80°$ for a range of $LT$ values (Matsuyama et al., 2006).

Matsuyama et al. (2007) also derived Eq. (A.29) by minimizing the total energy of the system in the case where elastic energy stored within the deformed lithosphere is ignored. Their derivation is an independent confirmation that the non-equilibrium inertia tensor governs the long-term stability of the rotation pole. [The extension to the case where elastic energy within the lithosphere is included in the minimization is also treated by Matsuyama et al. (2007).]

Finally, diagonalizing the total inertia tensor and combining the principal moments appropriately, yields the following expressions for the Stokes coefficients:

$$J_2 = k_f^T\frac{\Omega^2 a^3}{3GM} + \big(1+k_f^L\big)k_f^{T,*}Q'\frac{\Omega^2 a^3}{3GM}\left[\frac{1-3\cos^2\theta_L}{2}\right] - \big(k_f^{T,*}-k_f^T\big)\frac{\Omega^2 a^3}{3GM}\left[\frac{1-3\cos^2\delta}{2}\right], \tag{A.31}$$

and

$$4J_{22} = \big(1+k_f^L\big)k_f^{T,*}Q'\frac{\Omega^2 a^3}{3GM}\sin^2\theta_L$$

$$-\left(k_f^{T,*} - k_f^T\right)\frac{\Omega^2 a^3}{3GM}\sin^2\delta. \quad \text{(A.32)}$$

Note that when $Q' = 0$, $\delta = 0$ from Eq. (A.29); thus $J_2 = \Omega^2 a^3 k_f^{T,*}/(3GM)$ and $J_{22} = 0$, as required for the initial hydrostatic form of Fig. 1C1.

The appropriate value of $LT$ to be used in these expressions is the elastic thickness at the time Tharsis developed. Following the scenario shown in Fig. 1C, Eqs. (A.31) and (A.32) assume that TPW was driven by the formation of Tharsis alone, and that any change in $LT$ during this formation/TPW was negligible. If the latter was not the case, then the total remnant bulge would have to be computed by taking into account the changing pole position for each incremental change in $LT$. However, these expressions do not preclude that the elastic thickness continued to increase once TPW-driven by Tharsis ceased.

## References

Arkani-Hamed, J., Boutin, D., 2004. Paleomagnetic poles of Mars: Revisited. J. Geophys. Res. 109, doi:10.1029/2003JE002229. E03011.

Bills, B.G., James, T.S., 1999. Moments of inertia and rotational stability of Mars: Lithospheric support of subhydrostatic flattening. J. Geophys. Res. 104, 9081–9096.

Folkner, W.M., Yoder, C.F., Yuan, D.N., Standish, E.M., 1997. Internal structure and seasonal mass redistribution of Mars from radio tracking of Mars Pathfinder. Science 278, 1749–1752.

Gold, T., 1955. Instability of the Earth's axis of rotation. Nature 175, 526–529.

Hood, L.L., Young, C.N., Richmond, N.C., Harrison, K.P., 2005. Modeling of major martian magnetic anomalies: Further evidence for polar reorientations during the Noachian. Icarus 177, 144–173.

Matsuyama, I., Mitrovica, J.X., Manga, M., Perron, J.T., Richards, M.A., 2006. Rotational stability of dynamic planets with elastic lithospheres. J. Geophys. Res. 111, doi:10.1029/2005JE002447. E02003.

Matsuyama, I., Nimmo, F., Mitrovica, J.X., 2007. Reorientation of planets with lithospheres: The effect of elastic energy. Icarus 191, 401–412.

McGovern, P.J., Solomon, S.C., Smith, D.E., Zuber, M.T., Simons, M., Wieczorek, M.A., Phillips, R.J., Neumann, G.A., Aharonson, O., Head, J.W., 2004. Correction to "Localized gravity/topography admittance and correlation spectra on Mars: Implications for regional and global evolution". J. Geophys. Res. 109, doi:10.1029/2004JE002286. E07007.

Melosh, H.J., 1980. Tectonic patterns on a reoriented planet: Mars. Icarus 44, 745–751.

Mitrovica, J.X., Wahr, J., Matsuyama, I., Paulson, A., 2005. The rotational stability of an ice-age Earth. Geophys. J. Int. 161, 491–506.

Mound, J.E., Mitrovica, J.X., Forte, A.M., 2003. The equilibrium form of a rotating Earth with an elastic shell. Geophys. J. Int. 152, 237–241.

Munk, W., MacDonald, G.J.F., 1960. The Rotation of the Earth. Cambridge Univ. Press, Cambridge, UK.

Mutch, T.A., Arvidson, R.E., Head, J.W., Jones, K.L., Saunders, R.S., 1976. The Geology of Mars. Princeton Univ. Press, Princeton, NJ.

Peltier, W.R., 1974. The impulse response of a Maxwell Earth. Rev. Geophys. 12, 649–669.

Ricard, Y., Spada, G., Sabadini, R., 1993. Polar wandering of a dynamic Earth. Geophys. J. Int. 113, 284–298.

Schultz, P.H., Lutz, A.B., 1988. Polar wandering of Mars. Icarus 73, 91–141.

Schultz, P.H., Lutz-Garihan, A.B., 1982. Grazing impacts on Mars: A record of lost satellites. J. Geophys. Res. (Suppl. Ser.) 87, A84–A96.

Smith, D.E., Sjogren, W.L., Tyler, G.L., Balmino, G., Lemoine, F.G., Konopliv, A.S., 1999. The gravity field of Mars: Results of the Mars Global Surveyor. Science 286, 94–97.

Sohl, F., Spohn, T., 1997. The interior structure of Mars: Implications from SNC meteorites. J. Geophys. Res. 102, 1613–1636.

Sprenke, K.F., Baker, L.L., Williams, A.F., 2005. Polar wander on Mars: Evidence in the geoid. Icarus 174, 486–489.

Turcotte, D.L., Shcherbakov, B.D., Malamud, B.D., Kucinskas, A.B., 2002. Is the martian crust also the martian elastic lithosphere? J. Geophys. Res. 107 (E11), doi:10.1029/2001JE001594. 5091.

Wieczorek, M.A., Greff-Lefftz, M., Labrosse, S., van Thienen, P., Rouby, H., Besse, J., Feldman, W.C., 2005. The case for a martian inertial interchange true polar wander event. Lunar Planet. Sci. XXXVI. Abstract 1679.

Willemann, R.J., 1984. Reorientation of planets with elastic lithospheres. Icarus 60, 701–709.

Yoder, C.F., Konopliv, A.S., Yuan, D.N., Standish, E.M., 2003. Fluid core size of Mars from detection of the solar tide. Science 300, 299–303.

Zhong, S., Roberts, J.H., 2003. On the support of the Tharsis rise on Mars. Earth Planet. Sci. Lett. 214, 1–9.

Zuber, M.T., Smith, D.E., 1997. Mars without Tharsis. J. Geophys. Res. 102, 28673–28685.